Preprint
UCRL-JC-145410

Vapor-Deposited Polyimide Ablators for NIF: Effects of Deposition Process Parameters and Solvent Vapor Smoothing on Capsule Surface Finish

S.A. Letts, A.E.H. Nissen, P.J. Orthion, S.R. Buckley, E. Fearon, C. Chancellor, C.C. Roberts, B.K. Parrish and R.C. Cook

This article was submitted to Fusion Technology

U.S. Department of Energy
Lawrence Livermore National Laboratory

September 6, 2001

DISCLAIMER

VAPOR-DEPOSITED POLYIMIDE ABLATORS FOR NIF: EFFECTS OF DEPOSITION PROCESS PARAMETERS AND SOLVENT VAPOR SMOOTHING ON CAPSULE SURFACE FINISH

Stephan A. Letts, April E. H. Nissen, Pascal J. Orthion,
Steven R. Buckley, Evelyn Fearon, Christopher Chancellor,
C. Chad Roberts, Bryan K. Parrish and Robert C. Cook
Lawrence Livermore National Laboratory
P.O. Box 808, L-474
Livermore, CA 94551

Abstract

Over the last five years, LLNL has developed polyimide vapor deposition technology to coat ICF targets for NIF. One target design calls for 160-μm thick, smooth, uniform, vapor deposited polyimide (PI) coatings. Several physical properties of PI make it attractive for use as an ablator, including: reasonable DT permeability, high density, radiation stability, high tensile strength, and optical access to the DT ice layer. The smoothness of the PI coatings is a design requirement and has been a focus of our recent work. The coating conditions were evaluated to determine the effect on the coating surface finish. The most important factors that impact surface finish include mandrel quality, monomer mixing, self-shadowing, and abrasion. We have shown that high rate deposition (above 10 μm/h) is effective at reducing roughness. We believe this is due to the shorter total time the shell is agitated in the bouncer pan. By adjusting the coating conditions, coatings up to 160 μm thick are routinely made with a 300 nm RMS. Improvements in the bouncer pan technique have reduced roughness to about 50 nm RMS. Solvent vapor smoothing, a new technique also developed at LLNL, further improves the surface to 30 nm RMS.

Introduction

Polyimide continues to be one of the leading ablator design options for National Ignition Facility (NIF) ignition capsules.[1,2] At LLNL this option has been developed[3,4] using a monomer vapor deposition technique developed initially for thin flat coatings by Salem *et al.*[5] Related work has been pursued at LLE;[6,7,8,9] however, the goal of that work is very thin layers for direct drive capsules in contrast to our work to prepare the 150 μm thick layers required by the indirect drive designs.

In our previous reports[3,4] we detailed the basic procedures and coater equipment and will only briefly review the essential features below. We have demonstrated that full thickness layers could be deposited on GDP mandrels[10] and imidized to give uniform polyimide ablators; however, the surface finish of the capsules was poor. To remedy this problem we described a promising new vapor smoothing technique.

In the work presented here we describe our progress since the last report. The work will be divided into two parts. We will first discuss our studies to improve the quality of the "as-coated" shells. This work has involved both

detailed studies of certain aspects of defect generation in the coating as well as more process-oriented modifications. Following this we will detail our work on the vapor smoothing process which has involved both empirical studies of the effects of process variations on the effectiveness of the smoothing treatment as well as independent studies designed to better understand the smoothing mechanism.

Vapor deposition

Background

The first step in the fabrication of polyimide shells is the deposition of two monomeric substances, 4,4–oxydianiline (ODA) and pyromellitic dianhydride (PMDA), onto an agitated mandrel under high vacuum (10^{-6} torr). The monomers are placed in separate Knudsen cell[11] evaporators, and the two evaporators are heated to different temperatures during deposition in order to control their individual fluxes and maintain the desired 1:1 stoichiometry. A cartoon schematic of the fabrication process is shown in Figure 1. As the deposition proceeds it is expected that there is some level of reaction between the two monomers on the shell surface to form poly(amic acid) (PAA) as shown in Figure 2. However, the degree of polymerization is likely to be very low due to the solid phase of the coating and the concurrent lack of mobility. This view has been tentatively confirmed through MALDI measurements where primarily only dimers and trimers were seen.[12]

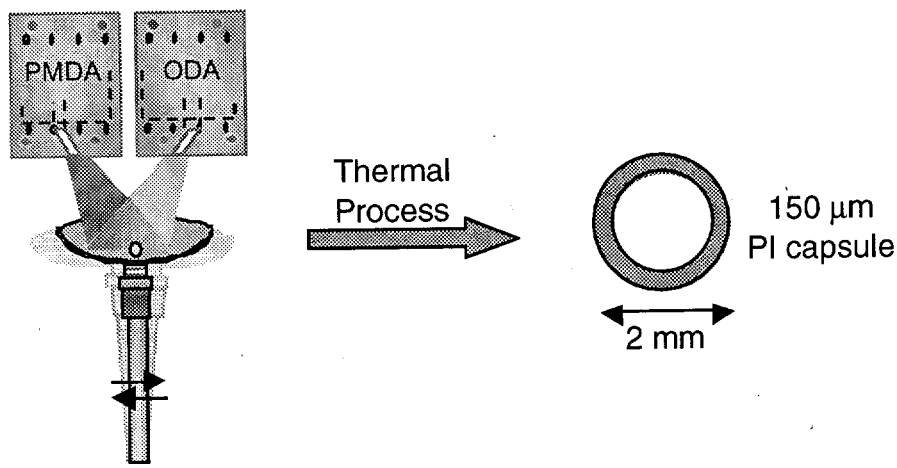

Figure 1. Diagram of the polyimide vapor deposition system.

Deposition process development

We have been using GDP mandrels[10] supplied by General Atomics, most of which have been prepared from batches of PαMS mandrels with some surface debris.[13] In what follows we designate these as "regular–batch" mandrels. These mandrels have good sphericity but a fine crust of small bumps all over the surface resulting in significant high mode roughness. Mandrels prepared from an unusually smooth PαMS mandrel batch are designated as "good–batch"

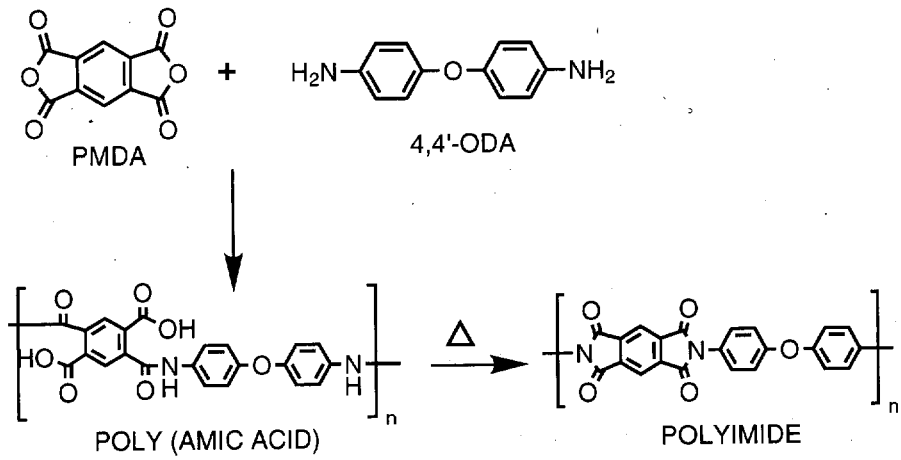

Figure 2. Diagram of the PMDA-ODA deposition reaction, followed by the ring closure with heat to the polyimide form.

mandrels. These shells are significantly smoother in the higher modes than typical batches, though the low mode sphericity is not as good.

To estimate the role of the starting mandrel on the final coating quality, we overcoated both good–batch mandrels and regular–batch mandrels under the same conditions with approximately 50 μm of coating. For these experiments, the deposition rate on the shells was about 2 μm/h. WYKO interferometric surface profilometer pictures of the as–coated shells before smoothing have been compared along with power spectra after smoothing, obtained from both SphereMapper and WYKO data.

Figure 3 shows 24.5X WYKO scans (191 x 251 μm) for a regular–batch mandrel with 46.3 μm of PAA and a good–batch mandrel coated with 41.2 μm of PAA. The differences in terms of number and height of defects are clear. The average RMS roughnesses (based on three views per shell) are 109 nm for the regular–batch mandrel while only 23 nm for the good–batch mandrel. The WYKO–based RMS values for the bare regular–batch and good–batch mandrels

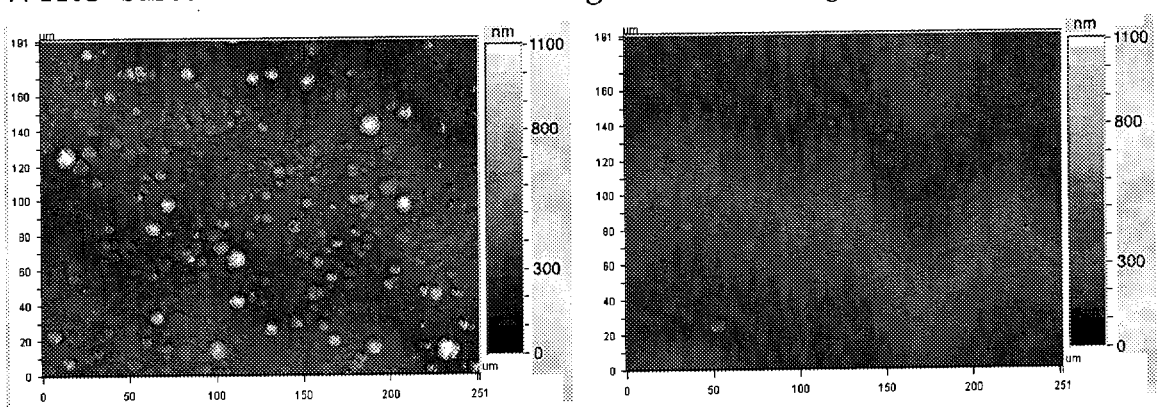

Figure 3. Regular–batch mandrel overcoated with 46.3 μm of PAA (left) and good–batch mandrel overcoated with 41.2 μm of PAA (right). Average RMS surface roughnesses are 109.0 nm and 23.0 nm, respectively.

were 23 and 8 nm, respectively. In Figure 4 we show the power spectra (calculated from WYKO[14] as well as SphereMapper data) for these shells after smoothing.

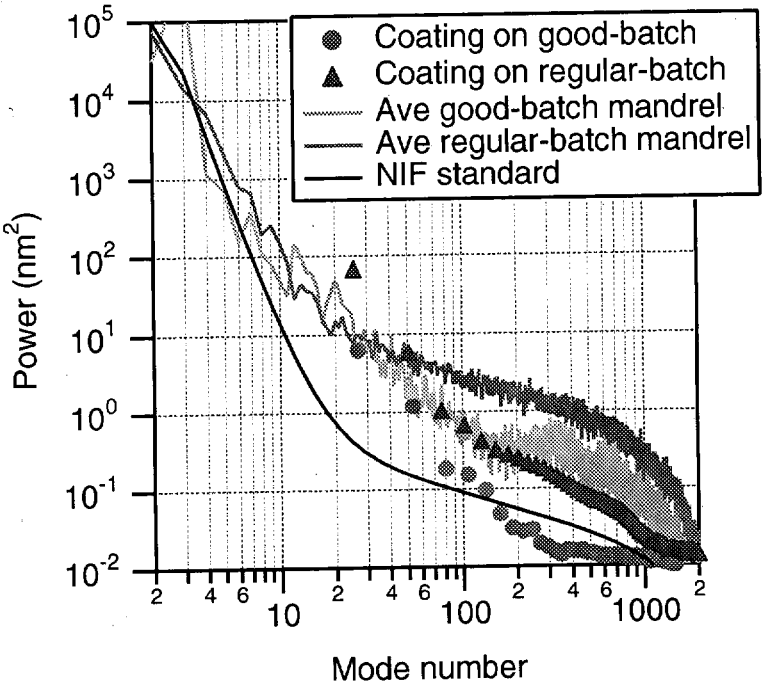

Figure 4. Smoothed shell WYKO–derived power spectra for coatings on a good–batch mandrel (41.2 μm thick) and a regular–batch mandrel (46.3 μm thick). The mandrel power spectra (SphereMapper) are also shown, as well as the NIF standard.

The effect of the mandrel surface finish is made obvious by the WYKO images of the as–coated shells, as the rougher mandrel leads to a coating with many bumps and a 5–times increase in RMS roughness. While the as–coated roughness is decreased by the smoothing process, more residual roughness is left on the final coating of the regular–batch mandrel, as compared to the good–batch mandrel in the power spectra. This is especially evident at the higher modes. Thus, using the smoothest mandrels possible will lead to the best polyimide coatings.

Past experiments[3] have revealed that the contact between the shell and the shaking pan was creating additional defects by either abrasion or adhesion phenomena. Hence, the deposition time is adversely correlated with the surface finish of the as–coated shell. Decreasing the deposition time is a possible pathway to improve the surface finish and can be achieved by increasing the deposition rate. Over the past 2 years, we have routinely coated mandrels at 1 μm/h and 2 μm/h. Recently we pushed the deposition rate to 10 μm/h, and the results we obtained are discussed below.

A mandrel coated with 140.9 μm at 2 μm/h shows a rougher surface finish after coating than a mandrel coated with 186.4 μm at 10 μm/h (Figure 5). In this

case, at 2 μm/h, the average RMS roughness (based on three shell views) is 1400 nm, where at 10 μm/h the average RMS value is 328 nm. Note the taller defects generated at 2 μm/h, up to 8.0 μm in height.

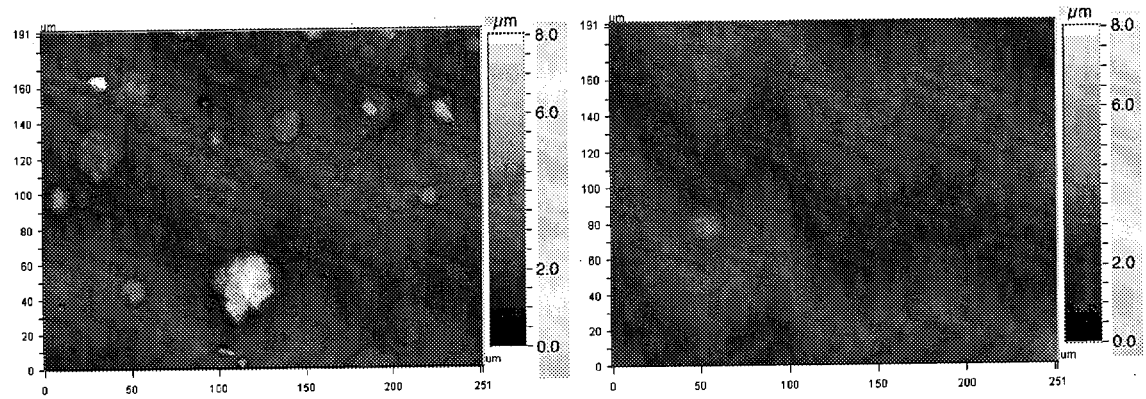

Figure 5. CH mandrel overcoated with 140.9 μm of PAA at 2 μm/h (left) and CH mandrel overcoated with 186.4 μm of PAA at 10 μm/h (right). Average RMS surface roughnesses are 1400 nm and 328 nm respectively.

Defect Growth from Particles

While we have empirically determined coating conditions to reduce the roughness of the deposited PAA coatings, we have also conducted experiments to determine the source of surface defects and possible routes to avoid defect generation.

To better understand the effect of substrate roughness on coating roughness, we studied the structure of coating defects growing from particles on the substrate, using glass slides as test substrates. We found that the coating thickness on a flat substrate has a bell shaped distribution with radial distance from the center of the coater. The coating thickness is a function of the evaporator operating temperatures (flux), substrate temperature, and the distance to the substrate. Examining the glass slides in a microscope we observed many coating defects caused by small particles on the substrate. The defects, shown in Figure 6, were found to have the outer surface bump displaced laterally from the originating dust particle. The distance from the surface bump to its substrate origin was determined with a measuring optical microscope. The defects near one evaporator were found to tilt toward the opposite evaporator. The angular tilt of the defect was found to be dependent on the substrate position.

Defects near the center of the coater are nearly vertical. Defects further from the center incline at increasing angles. We believe the surface growth direction is a function of the evaporator flux. The deposition of a monomer molecule results in polymer surface growth only if it is able to react with the opposite co-monomer species. The direction of film growth, which is directly related to the tilt of defects, is determined by the limiting reactant. Hence, under the ODA evaporator, the defects and surface growth direction is toward the PMDA evaporator. The surface is flooded with an excess of ODA but surface growth takes place only when the limiting reactant, PMDA, is supplied.

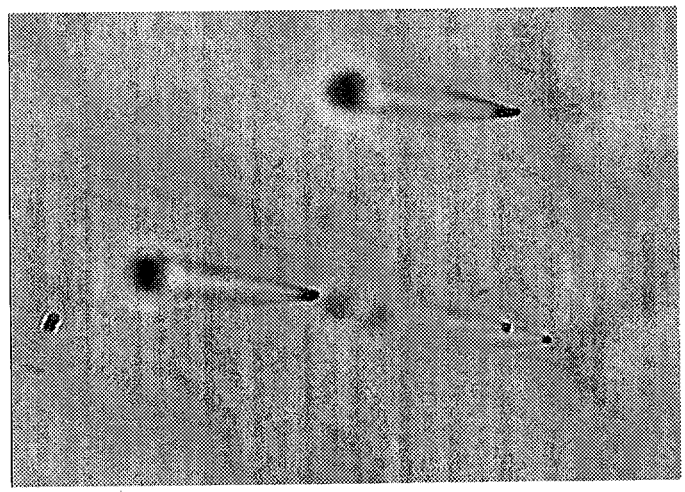

Figure 6. Defects in polyimide coatings done on flat substrates originate at particles and slant toward the limiting reactant monomer evaporator. The defects shown are 40 mm from the center on the ODA side. The coating thickness is 36 μm. The microscope is focused on the originating particle in the film. The outer surface bump is above the focal plane and consequently out of focus.

Monomers that do not react may desorb by evaporation into the vacuum system or may form crystals by joining with like molecules. The formation of crystals may be related to the deposition rate, the re-emission rate and the stoichiometry. Surface exposed to high rate and imbalanced stoichiometry may be more likely to incorporate crystals in the deposited coating.

Contact-free Coating of Shells

To study shell coating without the mechanical interference of a bouncer pan, we mounted shells on stalks and rotated them in the center of the coating chamber in the same position they would occupy if placed in a pan. During each coating run, two shells were held in orthogonal orientations (shown in Figure 7): one vertically, the other horizontally. It was expected that the equator of the horizontal shell would show the best surface finish obtainable without pan contact. The shells were coated at 1 to 4 μm/h rates. This resulted in a coating thickness from 15 to 60 μm on the pole of the vertical shell with the amount on the sides dropping off as a function of angle to the vertical as expected. On the horizontal shell the coating thickness around the equator was 10 to 40 μm.

The surface roughnesses of the two shells were measured with the WYKO interferometer. The pole of the shell rotated on a vertical axis had a roughness of about 57 nm RMS. However the side of the vertical shell has a roughness of 350 nm RMS. A rather sharp change in surface quality occurred at an angle of 53 degrees from the vertical. This corresponded to the limiting position where the surface is visible to both evaporator nozzles (monomer sources) at all times, thus insuring continuous mixed monomer deposition. It is conjectured that the increased roughness below this point may be due to momentary shadowing of the surface from one monomer source, resulting in deposition of only a single monomer and simultaneous crystallization.

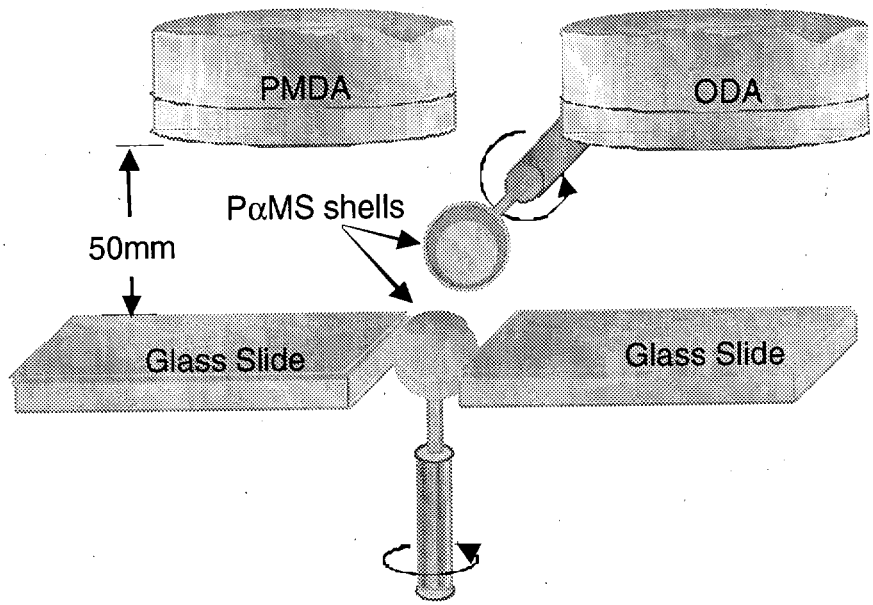

Figure 7. Rotated shells were coated in a vertical and horizontal orientation. Slides were placed at the side to measure the coating rate and surface roughness.

The equator band of the horizontal shell had a roughness of 123 nm RMS. In this case a portion of the equator was always subject to shadowing as described above. One possible explanation of the roughness in either orientation could be related to effects due to roughness from glancing angle deposition, an effect reported in single component deposition.[15,16] As will be shown below, this is not the case for our depositions. In the results just described the vertical shell was rotated at 22 RPM while the horizontal shell was rotated at 80 RPM. When the rate of shell rotation was reduced by a factor of 10, which would result in longer periods of shadowing, we found the magnitude of coating roughness doubled for the horizontal orientation and was unchanged at the pole of the vertical orientation, consistent with the shadowing argument.

To more carefully study the effect of stoichiometric imbalance caused by shadowing, we developed an approach to independently examine the effect of deposition rate and shadow time on surface roughness. We used a single 100-mm diameter silicon wafer as a substrate and mounted it horizontally on a rotating platform under the evaporators. Each monomer was constrained to coat only on one half of the wafer at any instant by placing a barrier between the evaporators. The substrate was rotated under the evaporators receiving alternate exposures to each of the monomers.

We found that slow rotation and fast deposition, conditions consistent with thicker single monomer layers, tended to produce rough surfaces that had obvious crystal inclusions. Rotating faster or depositing slower produced very smooth coatings. Table 1 summarizes the rough (R) and smooth (S) results in this series of experiments. The thickness of each individual monomer deposited per revolution (T_s) that results in smooth coating was calculated using the measured deposition rate. The thickness limit for smooth deposition is in the range of approximately 4 Å, which is less than a monolayer of monomer coverage.

Monomer layers thicker than 4 Å tend to crystallize. Based on this, to achieve smooth coatings on a shell held in a bouncer pan, the shell rotation must be fast enough to limit single monomer deposition in a region to less than 4 Å to prevent growth of monomer crystals.

Dep Rate	**Rotation Rate** (RPM)				**Ind. Monomer**
(μm/h)	30	100	200	400	T_s (Å/Rev)
4.2	R	S	-	-	3.5
10.3	-	R	S	-	4.3
16.3	-	R	-	S	3.4

Table 1. Summary of experiments on rotated flats and separated monomers.

From our investigations, we have begun to understand the source of defects that form on the shell surface during coating. Though we have tried to minimize defect formation due to bouncer agitation and other mechanical disturbances, even shells coated in a contact–free environment form surface defects, caused by shadowing and crystal formation due to the curvature of the mandrel. Thus a secondary post-coating treatment is necessary to achieve the desired surface finish.

Vapor smoothing

Overview of the smoothing process

In order to form PI the as–coated capsules must be heated to approximately 300°C to split out water and close the ring as shown in Figure 2. In our initial studies this was successfully accomplished in a tube furnace. However, the surface finish of the as–coated shells was very poor, and the simple imidization process maintained this poor finish. Even with the improvements we have made to the surface finish of the PAA coated shells through coating conditions as described above, the surface finish did not meet NIF specifications. As briefly reported previously,[3] we developed a preimidization smoothing process as shown in Figure 8. The as–coated shell is supported on a near room temperature N_2 flow that contains dimethyl sulfoxide (DMSO) vapor. The rough shell absorbs vapor from the flow, softening and perhaps fluidizing the PAA coating. After exposing the shell to smoothing vapors for a period of time, the temperature of the housing around the shell is increased to 300°C to imidize the smoothed layer while the shell is still levitated. The net result is that there appears to be surface tension driven flow on the surface, dramatically smoothing the very rough surface, at least over high frequencies.

We find in general that the surface finish of the final smoothed shell depends upon the degree of roughness present on the as–coated shell. The results from WYKO interferometry analysis for two examples of smoothing can be found in Figure 8. For coatings of about 70 μm thick, or approximately half of

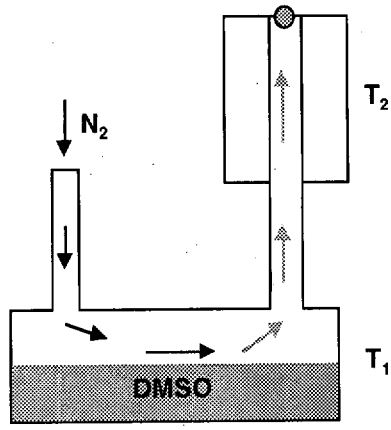

Figure 8. Diagram of the smoothing apparatus.

NIF thickness, the surface finish of the as–coated shell is made up of a large number of smaller bumps, with diameters less than 15 μm and heights less than 1 μm. The surface in Figure 9 is a particularly smooth example of coatings at this thickness, but the overall morphology is typical. This type of surface morphology is affected strongly by the smoothing process, and the final PI surface is quite smooth. For NIF scale coatings (150 μm or more), the as-coated surface has fewer bumps than thinner coatings, but the bumps are much larger:

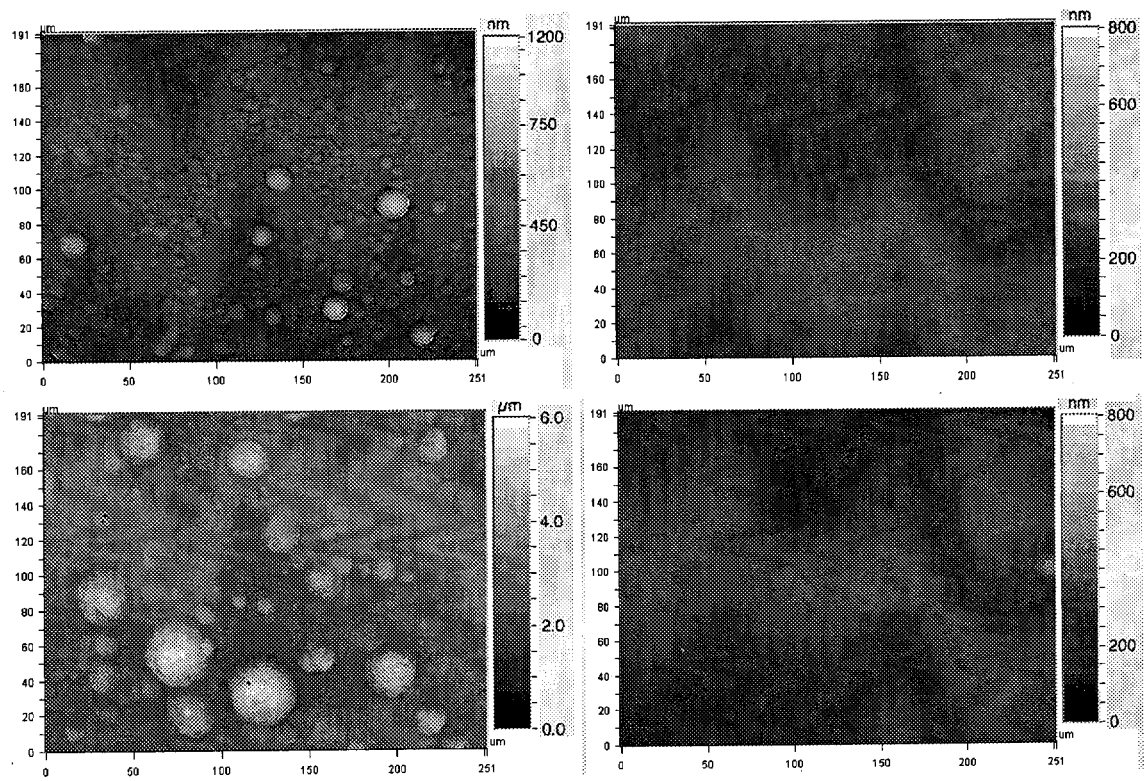

Figure 9. WYKO images (25X) for PAA coated shells, before (left) and after (right) smoothing. Top images are for 70 μm coating; bottom images are for 155 μm coating. Average RMS values are (clockwise from top left): 73 nm, 22 nm, 32 nm, and 457 nm.

20 μm in diameter and 3 μm in height. A surface with this morphology also becomes quite smooth after solvent exposure, but more subtle texture is left on the surface.

SphereMapping of these shells provides more information than WYKO analysis about the modal structure of the shell, especially at the lower modes. Power spectra for two sets of experiments can be found in Figures 10 and 11. For all thicknesses, the smoothing effect begins around mode 20, and is not typically effective at lower modes. However, as suggested by the WYKO images, coatings of different thicknesses are smoothed differently. For thinner coatings of about 50 μm (Figure 10), the shell shows greater roughness than the mandrel at modes above 10. The smoothing process removes most of this roughness, and the final shell is actually smoother than the mandrel at modes above 100.

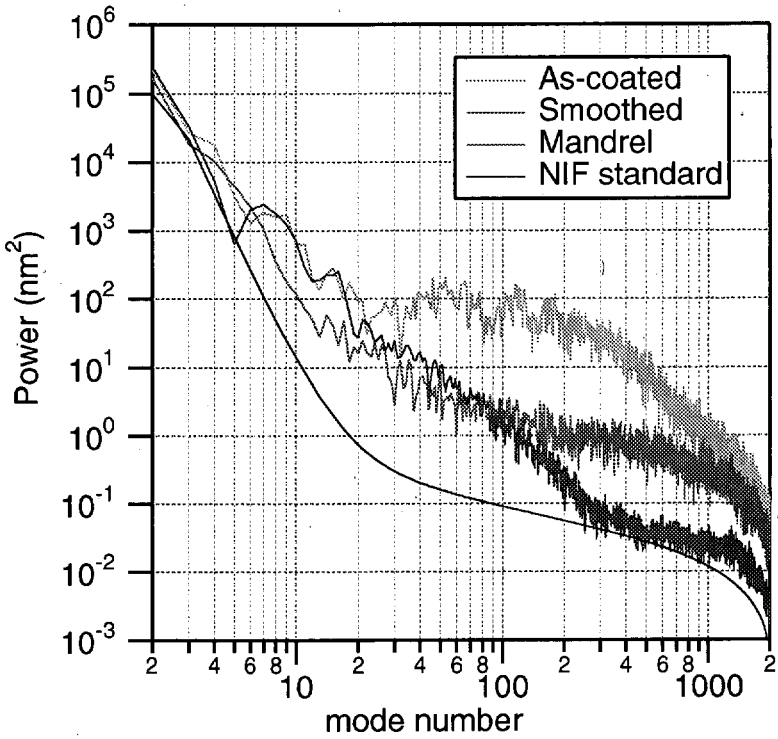

Figure 10. Power spectra for a bare mandrel, PAA coated shell, and smoothed PI shell, with 50 μm of coating.

As noted before, NIF scale coatings do not become as smooth. As seen in Figure 11, the as-coated shell is much rougher than shells with thinner coatings. Thus, while the smoothing process is still somewhat effective, and in fact creates a shell smoother than the mandrel at high modes, the shell still maintains roughness in the middle modes. Overall, the smoothing process appears to more effectively reduce power at almost all modes on thinner coatings.

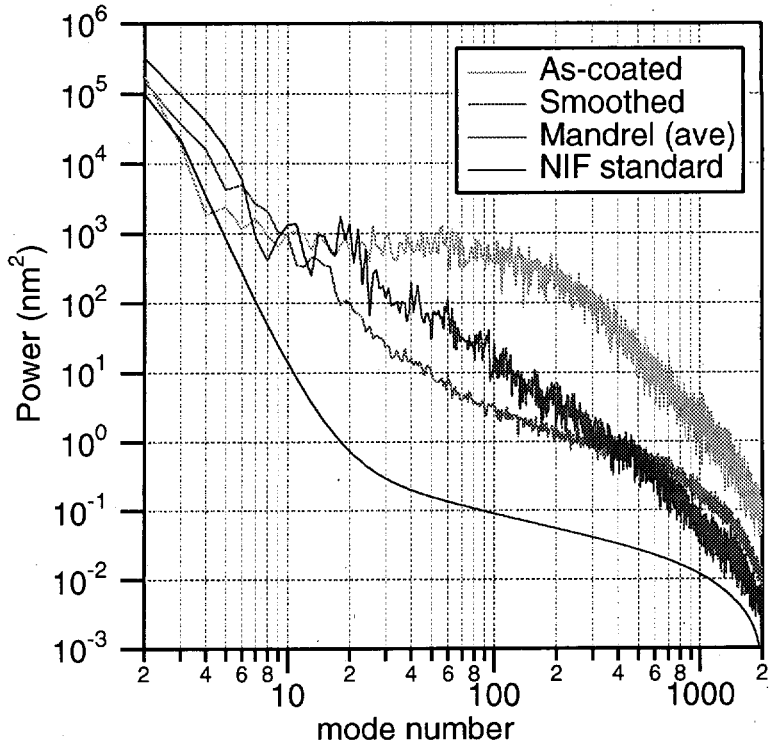

Figure 11. Power spectra for a bare mandrel, PAA-coated shell, and final smoothed shell, with 155 μm of coating.

Effect of smoothing process conditions

Several experiments were conducted to investigate the effect of solvent exposure time and solvent vapor concentration on the smoothing effectiveness. Shells from the same PAA coating batch were treated with the smoothing process, varying either the time of solvent exposure from 30 to 120 minutes, or varying the solvent vapor concentration, which is controlled most directly by the temperature of the solvent reservoir (the gas flow rate is determined by the mass of the shell). The results of these experiments are seen in Figure 12.

As expected, both longer times and higher concentrations create shells with lower RMS roughness, due to the increased solvent uptake on the surface of the shell and more flow of the fluidized layer. However, increasing both the exposure time and solvent concentration in order to obtain an extremely smooth shell presents some problems. A fluid layer that is too thick could cause slumping of the coating. Also, we have found that shells exposed at higher solvent levels are more prone to macroscopic cracking during the curing phase of the smoothing process, though the basic cause is as yet not understood.

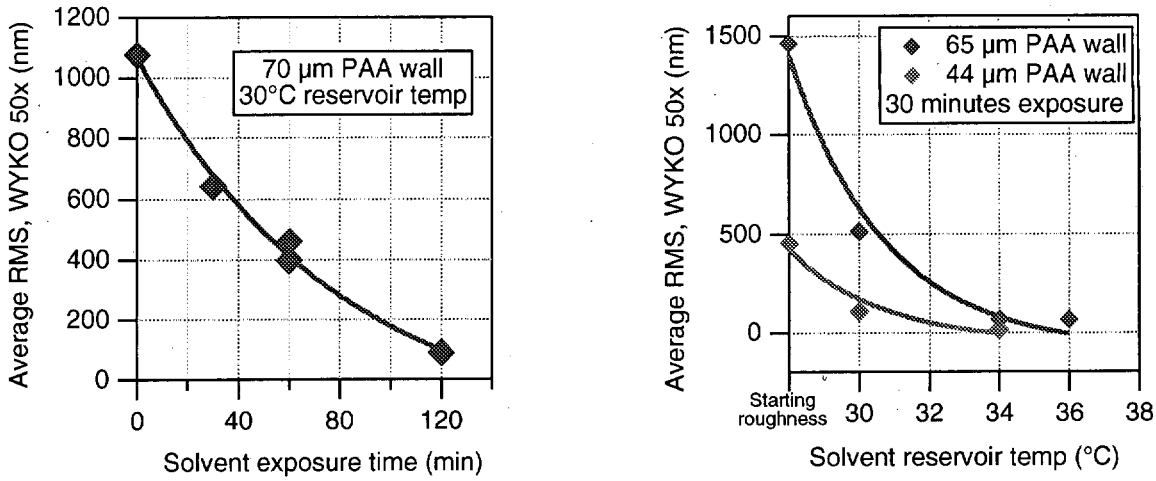

Figure 12. Change in RMS roughness, as measured by WYKO, on PAA shells as a function of solvent exposure time (left) and solvent reservoir temperature (right).

Smoothing time dependence investigations

To further explore the dependence of the smoothing process on both time and solvent concentration, experiments were designed to watch smoothing on the shell surface as it happens. A shell was placed in an enclosed cell under the WYKO objective, organic vapor was introduced to the cell, and the changes in morphology were measured over several hours. Because everything is at room temperature in this apparatus, the concentration of solvent was controlled by mixing of saturated solvent vapor with pure nitrogen gas.

The surface profile of bumps on the PAA surface changes dramatically with time. As shown in Figure 13, the bumps are flattened out as the surface fluidizes, and even two separated bumps (at 95 and 105 µm) flow into one. After 30 minutes, the surface is mostly flat, although further solvent exposure would continue to smooth the surface slightly. The WYKO data also provides power spectrum data (Figure 14) for modes 25 and above (limited by the patch size of the WYKO analysis). As one might expect, the higher modes are reduced first as the smallest defects are smoothed flat and the lower modes take much longer to begin smoothing and are not fully reduced even after 2 hours of solvent exposure. The changes in surface morphology during smoothing suggest surface tension-driven flow, as evidenced by both the movement of surface defects during smoothing, and the more rapid decrease in the higher modes of the power spectrum, where the defects with the highest amount of curvature are found. Efforts to exploit this surface tension effect are in progress.

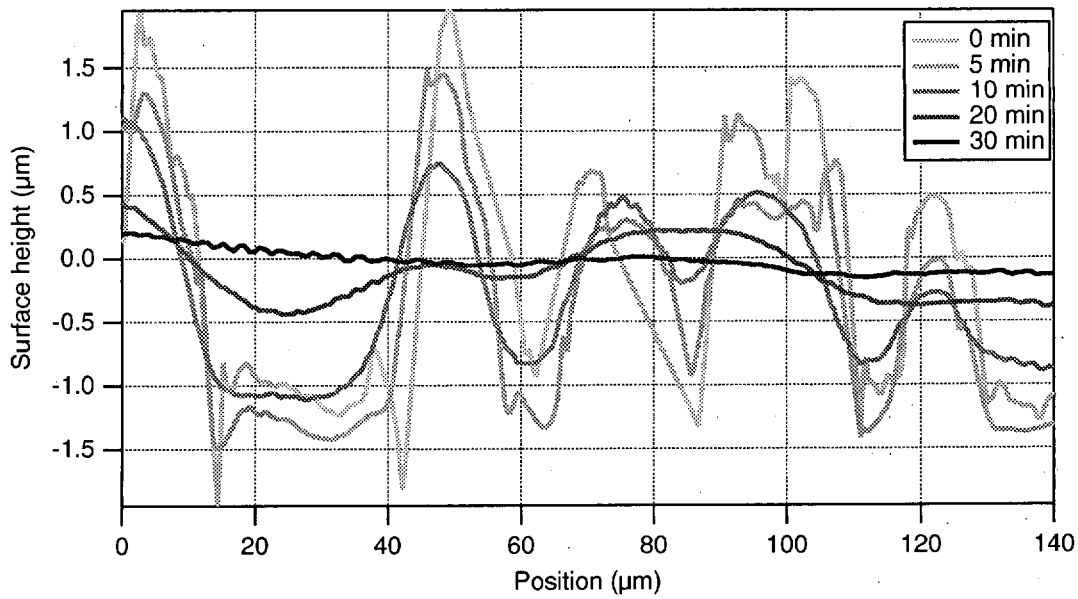

Figure 13. Line profile for smoothing of PAA surface over time, under WYKO analysis. Note the waves in the data at later times, which is due to an artifact of the interferometric method.

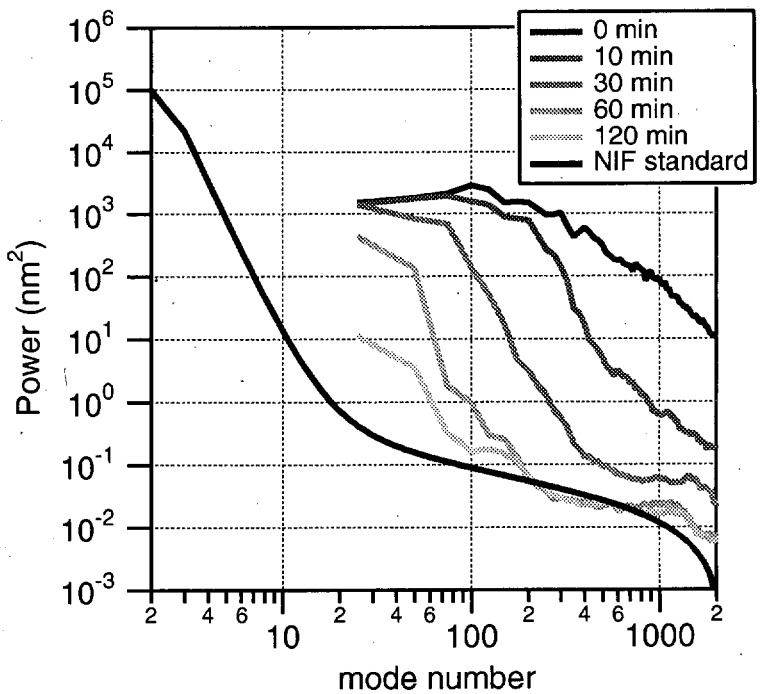

Figure 14. Change in WYKO power spectra as a function of solvent exposure time.

Discussion and Summary

Through our investigations, we have determined that the surface of the starting mandrel has a profound effect on the final coated surface, and the smoothing process is only partially effective at minimizing all surface defects. In an attempt to create the smoothest mandrel possible, one of our most recent approaches to achieve shells nearing the NIF specification is a step-coating method. With this approach, a CH mandrel would be coated with about 80 μm of PAA, and then treated with the smoothing process. The smoothed shell would then be used as a mandrel for a second PAA deposition, and smoothed once again. Step coating terminates the continuous growth of surface defects through the entire coating thickness and allows us to start with a fresh, very smooth mandrel at selected intervals through the deposition of coating.

Preliminary results are reported in Figure 15. After the first step, the shell is smoother than the as-coated shell, but the SphereMapper traces still reveal residual roughness, and the shell is rougher than the mandrel at all modes. This result after the first step is rougher at the higher modes than typically found for shells with coatings of similar thickness, but this should not adversely affect the second step. The second coating and smoothing step appears fill in and minimize many of the defects from the first coating, creating a much smoother surface. As seen in the power spectrum, improvements are made at almost all modes, including the lower to middle modes that are usually not affected by the smoothing process. This preliminary approach is hoped to prove a pathway to future success.

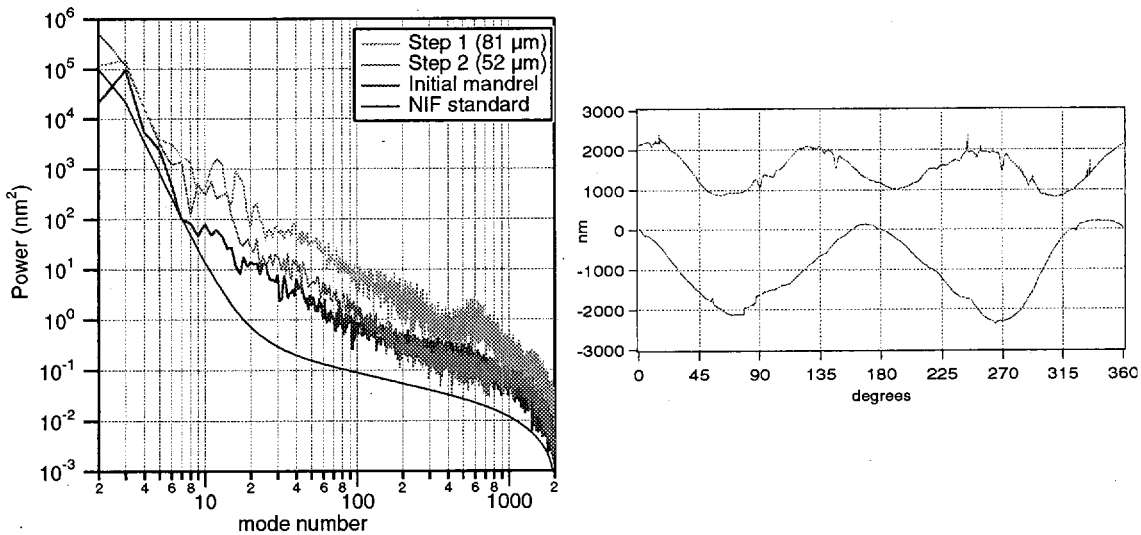

Figure 15. Preliminary results from step coating of PI shells, power spectra and SphereMapper traces, after the first (top) and second (bottom) steps.

This report outlines recent progress made in improving the surface finish of vapor deposited polyimide. We have shown that the coating surface roughness depends on a combination of several factors: initial roughness of the mandrel substrate, deposition rate and geometric shadowing during coating. To

meet the specifications set for NIF targets, some additional improvement is still needed. Recent work has shown that surface abrasion can be reduced using polymer pans and lower amplitude agitation, which has led to improved surface finish of the deposited poly(amic acid). To eliminate the effects of geometric shadowing, we are investigating the possibility of combining the two monomer streams in a mixing chamber to produce a single stream for deposition.

Acknowledgements

This work was performed under the auspices of the U.S. Department of Energy by the University of California, Lawrence Livermore National Laboratory under contract No. W-7405-Eng-48.

References

1. T. R. Dittrich, S. W. Haan, S. Pollaine, and A. K. Burnham, "NIF Capsule Design Update," *Fusion Technol.*, **31**, 402 (1997).

2. S. W. Haan, T. Dittrich, S. Hatchett, D. Hinkel, M. Marinak, D. Munro, O. Jones, S. Pollaine, and L. Suter, "Update on Ignition Target Fabrication Specifications," *Fusion Technol.*, this issue (2001).

3. C. C. Roberts, P. J. Orthion, A. E. Hassel, B. K. Parrish, S. R. Buckley, E. Fearon, S. A. Letts, and R. C. Cook, "Development of Polyimide Ablators for NIF," *Fusion Technol.*, **38**, 94 (2000).

4. C. C. Roberts, S. A. Letts, M. D. Saculla, E. J. Hsieh, and R. C. Cook, "Polyimide Films from Vapor Deposition: Toward High Strength NIF Capsules," *Fusion Technol.*, **35**, 138 (1999).

5. J. R. Salem, F. O. Sequeda, J. Duran, W. Y. Lee, and R. M. Yang, "Solventless Polyimide Films by Vapor Deposition," *J. Vac. Sci. Tech.*, **A4**, 369 (1986).

6. E. L. Alfonso, S.-H. Chen, R. Q. Gram, and D. R. Harding, "Fabrication of Polyimide Shells by Vapor Deposition for Use as ICF Targets," *Fusion Technol.*, **35**, 13 (1999).

7. F.-Y. Tsai, E. L. Alfonso, S.-H. Chen, and D. R. Harding, "Mechanical Properties and Gas Permeability of Polyimide Shells Fabricated by the Vapor Deposition Method," *Fusion Technol.*, **38**, 83 (2000).

8. F.-Y. Tsai, E. L. Alfonso, S.-H. Chen, and D. R. Harding, "Effects of Processing Conditions on the Quality and Properties of Vapor-Deposited Polyimide Shells," *Fusion Technol.*, this issue (2001).

9. E. L. Alfonso, S.-H. Chen, R. Q. Gram, and D. R. Harding, "Properties of polyimide shells made using vapor phase deposition," *J. Mater. Res.*, **13 (10)**, 2988 (1998).

10. B. W. McQuillian, A. Nikroo, D. A. Steinman, F. H. Elsner, D. G. Czechowicz, M. L. Hoppe, M. Sixtus, and W. J. Miller, "The PAMS/GDP Process for Production of ICF Target Mandrels," *Fusion Technol.*, **31**, 381 (1997).

11. C. W. Hutchings and M. Grunze, "Apparatus for chemical vapor deposition of polyimide films," *Rev. Sci. Instrum.*, **66 (7)**, 3943 (1995).

12. V. Malba, V. Liberman, and A. F. Bernhardt, "Vapor Deposition Polymerization of Polyimide for Microelectronic Applications," *J. Vac. Sci. Tech.*, **A15**, 844 (1997).

13. Better mandrels are now becoming available, see M. Takagi, "Development of high quality poly(α-methylstyrene) mandrels for NIF," *Fusion Technol.*, this issue (2001).

14. Software for WYKO power spectrum analysis developed by R. L. McEachern, LLNL.

15. S. K. Dew, T. Smy, and M. J. Brett, "Simulation of the Microstructure of Chemical Vapor Deposited Refractory Thin Films," *J. Vac. Sci. Tech.*, **B10**, 618 (1992).

16. G. S. Bales and A. Zangwill, "Macroscopic Model for Columnar Growth of Amorphous Films by Sputter Deposition," *J. Vac. Sci. Tech.*, **A9**, 145 (1991).